J|A|C|S
ARTICLES
Published on Web 05/26/2007

Direct Immobilization of Fab′ in Nanocapillaries for Manipulating Mass-Limited Samples

Bo Young Kim,[†] Carla B. Swearingen,[§] Ja-an A. Ho,[§] Elena V. Romanova,[†] Paul W. Bohn,[‡] and Jonathan V. Sweedler*,[†]

Contribution from the Department of Chemistry and Beckman Institute for Advanced Science and Technology, University of Illinois at Urbana-Champaign, 600 South Mathews, Urbana, Illinois 61801, and Department of Chemical and Biomolecular Engineering and Department of Chemistry, University of Notre Dame, Notre Dame, Indiana 46556

Received January 3, 2007; E-mail: jsweedle@uiuc.edu

Abstract: Interfacing nanoscale elements into a microfluidic device enables a new range of fluidic manipulations. Nanocapillary array membranes (NCAMs), consisting of thin ($5\ \mu m < d < 20\ \mu m$) membranes containing arrays of nanometer diameter ($10\ nm < a < 500\ nm$) pores, are a convenient method of interfacing vertically separated microchannels in microfluidic devices that allow the external control of analyte transport between microfluidic channels. To add functionality to these nanopores beyond simple fluid transport, here we incorporate an antibody-based molecular recognition element onto the pore surface that allows selective capture, purification, and release of specific analytes from a mixture. The pores are fabricated by electroless plating of gold into the nanopores of an NCAM (Au-NCAM). An antibody is then immobilized on the Au-NCAM via gold-thiol chemistry as a thiolated fragment of antigen-binding (Fab′) prepared by direct digestion of the antibody followed by reduction of the disulfide linkage on the hinge region. The successful immobilization and biological activity of the resultant Fab′ through this protocol is verified on planar gold by fluorescence microscopy, scanning electron microscopy, and atomic force microscopy. Selective capture and release of human insulin is verified using matrix-assisted laser desorption/ionization time-of-flight mass spectrometry. The relative mass spectral peak intensities for insulin versus nonantigenic peptides increase more than 20-fold after passing through the Fab′-Au-NCAM relative to the control Au-NCAM. The affinity-tagged Au-NCAM can be incorporated into microfluidic devices to allow the concentration, capture, and characterization of analytes in complex mixtures with high specificity.

Introduction

Increased understanding of dynamic cellular events and cell-to-cell signaling can be greatly facilitated by advances in biotechnology and measurement sciences.[1,2] Demands for high-performance platforms capable of handling small amounts of complex samples are a driving force[3,4] in the development of microscale total analysis systems (μTAS).[5,6] In this work, we describe an approach for interfacing nanometer-scale capillaries (pores) that includes an affinity element for molecular recognition, capture, and release of a preselected analyte to microfluidic devices. The resulting nanocapillary array membranes (NCAMs) form intelligent, electrically switchable transport elements that connect physically separated microchannels.

Characterization of biological systems often requires sophisticated, multistep manipulations of mass-limited samples, placing extraordinary constraints on μTAS devices. Combining nanofluidics and microfluidics into an integrated, multitasking analysis platform constitutes one strategy for handling the challenges posed in these situations. Development of hybrid nanofluidic/microfluidic device structures has been pursued in several research laboratories to facilitate sample preparation, concentration, separation, and selective transport.[7−17] The multilevel, integrated microfluidic architectures utilized in these devices

[†] University of Illinois at Urbana-Champaign.
[‡] University of Notre Dame.
[§] Ja-an Annie Ho is currently at the Department of Chemistry, National Tsing Hua University, Hsin-chu, 30013 Taiwan. Carla Swearingen is at John Brown College, Siloam Springs, Arkansas.

(1) Whitesides, G. M. *Nat. Biotechnol.* **2003**, *21*, 1161.
(2) Hatcher, N. G.; Richmond, T. A.; Rubakhin, S. S.; Sweedler, J. V. *Anal. Chem.* **2005**, *77*, 1580.
(3) Bange, A.; Halsall, H. B.; Heineman, W. R. *Biosens. Bioelectron.* **2005**, *20*, 2488.
(4) Whitesides, G. M. *Nature* **2006**, *442*, 368.
(5) Dittrich, P. S.; Manz, A. *Anal. Bioanal. Chem.* **2005**, *382*, 1771.
(6) Janasek, D.; Franzke, J.; Manz, A. *Nature* **2006**, *442*, 374.
(7) Kuo, T. C.; Cannon, D. M.; Shannon, M. A.; Bohn, P. W.; Sweedler, J. V. *Sens. Actuators, A-Phys.* **2003**, *102*, 223.
(8) Kuo, T. C.; Cannon, D. M.; Chen, Y. N.; Tulock, J. J.; Shannon, M. A.; Sweedler, J. V.; Bohn, P. W. *Anal. Chem.* **2003**, *75*, 1861.
(9) Cannon, D. M.; Kuo, T. C.; Bohn, P. W.; Sweedler, J. V. *Anal. Chem.* **2003**, *75*, 2224.
(10) Kuo, T. C.; Kim, H. K.; Cannon, D. M.; Shannon, M. A.; Sweedler, J. V.; Bohn, P. W. *Angew. Chem., Int. Ed.* **2004**, *43*, 1862.
(11) Tulock, J. J.; Shannon, M. A.; Bohn, P. W.; Sweedler, J. V. *Anal. Chem.* **2004**, *76*, 6419.
(12) Fa, K.; Tulock, J. J.; Sweedler, J. V.; Bohn, P. W. *J. Am. Chem. Soc.* **2005**, *127*, 13928.
(13) Iannacone, J. M.; Jakubowski, J. A.; Bohn, P. W.; Sweedler, J. V. *Electrophoresis* **2005**, *26*, 4684.
(14) Wang, Y. C.; Stevens, A. L.; Han, J. *Anal. Chem.* **2005**, *77*, 4293.
(15) Hatch, A. V.; Herr, A. E.; Throckmorton, D. J.; Brennan, J. S.; Singh, A. K. *Anal. Chem.* **2006**, *78*, 4976.
(16) Albertorio, F.; Daniel, S.; Cremer, P. S. *J. Am. Chem. Soc.* **2006**, *128*, 7168.
(17) Fu, J. M., P.; Han, J. *Appl. Phys. Lett.* **2005**, *87*, 263902.1.

10.1021/ja070041w CCC: $37.00

exploit the unique electrokinetic flow properties of arrays of nanometer-scale pores as interconnects for spatially separated, three-dimensional microfluidic networks.[7−13] The critical physical parameter relevant to fluid flow at the nanoscale is the product of the nanocapillary diameter (a) and the inverse Debye length (κ), where κ is dependent on the ionic strength of the solution and determines the thickness of the electrical double layer.[18] Knowing these parameters allows one to predict the fluidic motion and the electrical bias to control the direction of flow.[19] For example, when $\kappa a \gg 1$, electrophoresis dominates nanocapillary transport, while electroosmosis dominates when $\kappa a \leq 1$.[12] Integration of NCAMs into microfluidic networks thus enables a unique set of fluidic and transport capabilities that support the concentration, multidimensional separation, transport, reactive processing, and conditioning of mass-limited samples.[7−13]

Beyond simple transport control, the NCAMs offer the possibility of synthetically elaborating the interior of the nanopores to effect chemical transformations at high efficiency. Antibodies (or immunoglobulin) are multimeric glycoproteins with highly specific molecular recognition abilities.[20] Because of this specificity, immobilization of antibodies (IgG) onto solid surfaces has been extensively studied.[21] When immobilizing an antibody on a solid support, it is critical to control its orientation, so that the antigen-binding site is exposed toward the fluid, and to preserve its molecular recognition ability. In addition, most popular antibody immobilization strategies exhibit unique challenges that should be overcome for successful implementation.[21,22] In the strategy used here, a fragment encompassing the antigen-binding region (Fab′) is produced by proteolytic cleavage of an intact IgG, followed by controlled reduction of disulfide linkages on the hinge region and spontaneous immobilization on gold with controlled orientation dictated by the gold-thiol interaction.[21,23,24] In addition to its straightforward immobilization, the utilization of Fab′ produces higher molecular density compared to the use of intact IgG molecules.[21,23]

Several groups have reported immobilizing functional biomolecules, including enzymes,[25−28] antibodies,[29] and nucleic acids,[30−32] into gold nanopores through gold-thiol chemistry, and these have been studied for differential chemical transport, separations,[33] and biological sensor applications.[34] Biomolecular recognition in nanopores has been accomplished with materials other than gold; for example, Lee et al.[35] immobilized Fab on silica nanotubes and demonstrated enantiomeric separation of 4-[3-(4-fluorophenyl)-2-hydroxy-1-[1,2,4]triazol-1-yl-propyl]-benzonitrile from a racemic mixture. The silica nanotubes were prepared by sol−gel synthesis by using an alumina membrane as a template and by immobilizing the Fab in the silica nanotubes through Schiff base formation.

Here, we fabricate gold nanopores within NCAMs, followed by immobilization of antibody fragments, to create an array of attoliter-volume molecular recognition chambers. Specifically, the molecular recognition capability for selective capture and release of specific antigens is prepared by immobilizing the Fab′ inside the Au-NCAM walls via gold-thiol chemistry. We use the monoclonal antibody to the insulin C-terminal and insulin to create a model antibody-based molecular recognition NCAM. Fab′ immobilization is verified on the planar gold surface as well as on the pore walls by fluorescence microscopy (FM), atomic force microscopy (AFM), and scanning electron microscopy (SEM). Matrix-assisted laser desorption/ionization (MALDI) mass spectrometry (MS) is then used to assess the ability of the NCAM-immobilized, antibody-based molecular recognition motif to trap and concentrate specific analytes and to release them on demand.

Experimental Section

The NCAMs used here consist of polycarbonate nuclear track-etched (PCTE) membranes from GE Osmonics (Minnetonka, MN) with polyvinylpyrrolidone coating. The following experimental details are listed in the Supporting Information: materials and reagents, buffers and MALDI matrix, planar gold substrate preparation for microscopy, electroless gold plating,[36] preparation of the thiolated Fab′ antibody fragment,[21] microscopic imaging of the Fab′-Au surface, and matrix-assisted laser desorption/ionization time-of-flight mass spectrometry (MALDI-TOF MS).

Results

Modifying the Planar Gold Surface and Au-NCAM with Fab′. Initially, it was important to verify the immobilization of biochemically competent Fab′ onto the gold surface and in the nanopores. This was done using a combination of optical, electron, and atomic force microscopies, as well as MS. Fab′ can be spontaneously immobilized onto the gold surface with orientation control, although there exists conflicting information in the literature regarding the viability of the resulting immunoreactive surface.[21] Therefore, before creating the antibody-based molecular recognition nanopore (Fab′-Au-NCAM), the construction strategy was validated on a planar gold surface. It has been reported that mouse monoclonal IgG1 is poorly digested by pepsin.[37,38] However, by extending the incubation time of the antibody with immobilized pepsin, successful results were obtained.

(18) Kemery, P. J.; Steehler, J. K.; Bohn, P. W. *Langmuir* **1998**, *14*, 2884.
(19) Kuo, T. C.; Sloan, L. A.; Sweedler, J. V.; Bohn, P. W. *Langmuir* **2001**, *17*, 6298.
(20) Corley, R. B., Antibodies. In *Immunology, Infection, and Immunity*; Pier, G. B., Lyczak, J. B., Wetzler, L. M., Eds.; ASM press: Washington, DC, 2004; pp 113.
(21) Brogan, K. L.; Wolfe, K. N.; Jones, P. A.; Schoenfisch, M. H. *Anal. Chim. Acta* **2003**, *496*, 73.
(22) Rao, S. V.; Anderson, K. W.; Bachas, L. G. *Mikrochim. Acta* **1998**, *128*, 127.
(23) O'Brien, J. C.; Jones, V. W.; Porter, M. D.; Mosher, C. L.; Henderson, E. *Anal. Chem.* **2000**, *72*, 703.
(24) Nuzzo, R. G.; Allara, D. L. *J. Am. Chem. Soc.* **1983**, *105*, 4481.
(25) Delvaux, M.; Demoustier-Champagne, S. *Biosens. Bioelectron.* **2003**, *18*, 943.
(26) Delvaux, M.; Demoustier-Champagne, S.; Walcarius, A. *Electroanalysis* **2004**, *16*, 190.
(27) Delvaux, M.; Walcarius, A.; Demoustier-Champagne, S. *Anal. Chim. Acta* **2004**, *525*, 221.
(28) Delvaux, M.; Walcarius, A.; Demoustier-Champagne, S. *Biosens. Bioelectron.* **2005**, *20*, 1587.
(29) Siwy, Z.; Trofin, L.; Kohli, P.; Baker, L. A.; Trautmann, C.; Martin, C. R. *J. Am. Chem. Soc.* **2005**, *127*, 5000.
(30) Wernette, D. P.; Swearingen, C. B.; Cropek, D. M.; Lu, Y.; Sweedler, J. V.; Bohn, P. W. *Analyst* **2006**, *131*, 41.
(31) Kohli, P.; Harrell, C. C.; Cao, Z.; Gasparac, R.; Tan, W.; Martin, C. R. *Science* **2004**, *305*, 984.
(32) Harrell, C. C.; Kohli, P.; Siwy, Z.; Martin, C. R. *J. Am. Chem. Soc.* **2004**, *126*, 15646.
(33) Wirtz, M.; Yu, S. F.; Martin, C. R. *Analyst* **2002**, *127*, 871.
(34) Kohli, P.; Wirtz, M.; Martin, C. R. *Electroanalysis* **2004**, *16*, 9.
(35) Lee, S. B.; Mitchell, D. T.; Trofin, L.; Nevanen, T. K.; Soderlund, H.; Martin, C. R. *Science* **2002**, *296*, 2198.
(36) Menon, V. P.; Martin, C. R. *Anal. Chem.* **1995**, *67*, 1920.
(37) Mariani, M.; Camagna, M.; Tarditi, L.; Seccamani, E. *Mol. Immunol.* **1991**, *28*, 69.
(38) Wilson, D. S.; Wu, J.; Peluso, P.; Nock, S. *J. Immunol. Methods* **2002**, *260*, 29.

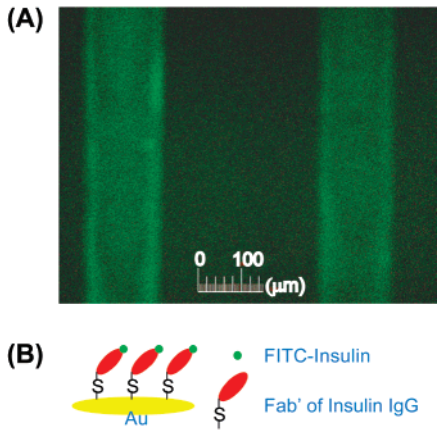

Figure 1. Fluorescence image of a Fab′-Au surface exposed to FITC-insulin. (A) FITC-insulin was selectively captured only on the Fab′-Au surface prepared by microfluidic patterning (green channels). (B) Schematic representation of the structure of the Fab′-Au surface with captured FITC-insulin.

The Fab′ was immobilized on planar gold by microfluidic patterning.[39] First, a poly(dimethylsiloxane) (PDMS) mask with microfluidic channels prepared by soft lithography and rapid prototyping[40] was placed onto a clean gold surface. Next, the prepared Fab′ solution filled the microfluidic channels and was incubated at 4 °C. After 38 h, the Fab′ solution in the microfluidic channels was replaced with phosphate buffered saline (PBS), the PDMS mask was peeled off from the gold surface, and the surface was immediately rinsed with copious amounts of PBS to prevent lateral spreading of the Fab′. The Fab′-Au surface was thoroughly washed with PBS containing 0.01%−0.05% Tween-2 (T/PBS) using a shaker. After washing, the Fab′-Au was put into the blocker for 1 h to prevent nonspecific adsorption of protein on the unmodified gold surface, and the surface was immediately immunoreacted with FITC-insulin for Fab′-Au imaging by fluorescence microscopy.

Figure 1A displays a fluorescence microscopic image taken to verify the activity of the Fab′-Au along with a schematic representation of the modified surface structure in Figure 1B. Because Fab′ was immobilized by microfluidic patterning[39] in four parallel 100 μm microfluidic channels prepared using rapid prototyping (two channels are shown in this image),[40] only the portion of the pattern in which immobilized Fab′ successfully captured fluorescein isothiocyanate (FITC)-insulin is visible; the intense fluorescence of these channels documents the activity of the immobilized Fab′.

While the fluorescence microscope image verifies antibody placement and biochemical function on the planar surface, the immobilization may be more difficult, and is certainly more difficult to validate, within the nanopore. Thus, several different approaches, including immunogold staining, were used to validate antibody function on the planar surface and in the pores. Experimental detail is described in the Supporting Information. Planar surfaces derivatized with the Au-IgG-Fab′-Au surface structure were prepared as illustrated in Figure 2D. Figure 2A shows an SEM image of the Au-IgG-Fab′-Au surface fabricated by microfluidic patterning on an ultraflat planar gold surface. The AFM-derived root-mean-square surface topographic variability of the freshly stripped gold surface before microfluidic patterning was 0.19 nm, which is close to the previously reported value (ca. 0.23 nm).[41] In Figure 2A, the contrast in the SEM image collected by the secondary electron (SE) detector reveals the microfluidic feature, UIUC, indicating that protein[42,43] is retained on the surface. Although SEM with secondary electron imaging is a sensitive, semiquantitative characterization tool for protein adsorption on a gold surface, the contrast in the image cannot provide details about the activity or orientation of the immobilized protein.[42,43] Therefore, a 3×3 μm^2 area on the feature (Figure 2B) was examined with AFM to determine if the difference in contrast in the SEM image resulted from functionally active immobilized protein. This was accomplished by looking for the gold particles on the Au-IgG that were bound to immobilized Fab′ on the gold surface. In the AFM height-mode image in Figure 2B, the bright spikes resulted from individual gold particles attached to the Au-IgG bound to the surface-immobilized Fab′. Figure 2C illustrates that the mea-

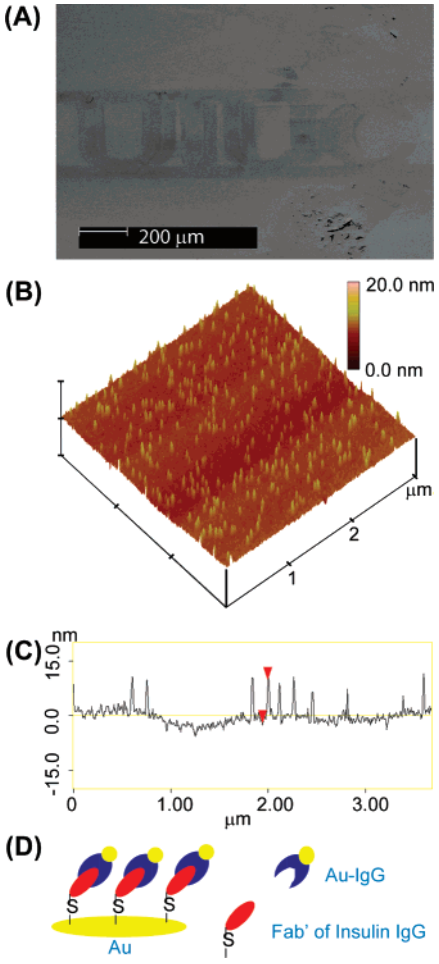

Figure 2. SEM and AFM images of a Au-IgG-Fab′-Au surface. (A) SEM image of Au-IgG-Fab′-Au. (B) AFM image of Au-IgG-Fab′-Au. Bright peaks indicate the 10 nm Au-IgG gold particles. (C) Section analysis of B in which the height of the excursions shows good agreement with the size of gold nanoparticles (diameter 10 nm). The distance between the two red triangles along the *y*-axis on C is 11.8 nm. (D) Schematic representation of the Au-IgG-Fab′-Au surface structure.

(39) Delamarche, E.; Bernard, A.; Schmid, H.; Michel, B.; Biebuyck, H. *Science* **1997**, *276*, 779.
(40) McDonald, J. C.; Duffy, D. C.; Anderson, J. R.; Chiu, D. T.; Wu, H. K.; Schueller, O. J. A.; Whitesides, G. M. *Electrophoresis* **2000**, *21*, 27.
(41) Blackstock, J. J.; Li, Z. Y.; Freeman, M. R.; Stewart, D. R. *Surf. Sci.* **2003**, *546*, 87.
(42) Lopez, G. P.; Biebuyck, H. A.; Harter, R.; Kumar, A.; Whitesides, G. M. *J. Am. Chem. Soc.* **1993**, *115*, 10774.
(43) Mack, N. H.; Dong, R.; Nuzzo, R. G. *J. Am. Chem. Soc.* **2006**, *128*, 7871.

sured peak height is in good agreement with the diameter (10 nm) of the gold particles. The measured particle density was 54.1 particles/μm^2 (485 particles within the scanned area) when the threshold parameters were set to yield a mean peak height of 9.05 nm. When a 3×3 μm^2 area of control surface (blocked with the PDMS mask during Fab′ immobilization) was scanned, less than 10 particles were observed within the scanned area (see Supporting Information). Thus, the successful attachment of functional antibody to the planar surface was demonstrated.

Characterization of immobilized antibody fragments within the nanopore presents additional challenges. NCAMs with an antibody-based molecular recognition motif (Fab′-Au-NCAM) were constructed on a Au-NCAM prepared via electroless plating of the PCTE membranes. The advantage of electroless plating is that, in contrast to electrodeposition, it does not require a conductive substrate, so that the gold can be coated on and in the NCAMs.[36] Controlling the kinetics of the homogeneous electron-transfer reaction is important to reduce the Au precursor ions on the substrate rather than in solution.[36] Figure 3 shows SEM images of NCAMs with an initial pore diameter of 200 nm, with and without gold on the membranes. As observed in the SEM images, electroless plating produces a rough microscopic surface, resulting in a large effective surface area for immobilization of functional molecules. In Figure 3B, the dark areas indicate the absence of gold. Because the image was collected by the backscattered electron (BSE) detector, the higher atomic number element appears brighter in the image. In this case, the phase contrast is based on gold versus carbon, the major element of the NCAM. However, the absence of gold on the surface did not necessarily correspond to a pore entrance. Therefore, to examine whether or not the pore entrances were clogged after electroless plating, the gold on the NCAM surface was removed, cf. Figure 3C. The specimen reveals open pores as bright rings in the BSE image. The pore-entrance diameter on the Au-NCAM is approximately 100 nm, illustrating the expected decrease in pore diameter upon electroless gold deposition. The visible halos around the rings indicate that the nanocapillaries were not always aligned at a 90° angle from the surface. It has been suggested that the "nonideal" pore geometry is due to the damage track by secondary electrons produced by the fission fragment while it is generating the damage track on the polycarbonate.[44] Figure 3D displays a cross section of a Au-NCAM prepared by breaking wet Au-NCAMs in liquid nitrogen, showing the well-defined, gold-lined cylindrical pores within the polycarbonate framework.

An antibody-based, molecular-recognition NCAM (Au-IgG-Fab′-Au-NCAM) is shown in Figure 4A. Fab′ immobilizations on Au-NCAMs were prepared essentially in the same way as the Fab′-Au samples. For better imaging, larger 600 nm pore PCTE membranes were used for sample preparation rather than the 200 nm pore membranes used for selective capture and release of antigen. Au-NCAMs prepared from the 600 nm PCTE membranes produced approximately 500 nm diameter pores. To image the inner pore surface, Au-IgG-Fab′-Au-NCAMs and control Au-NCAMs were broken in liquid nitrogen after treatment with fixative and rinsing in DI water. Next, the membranes were examined for internal nanocapillary features (the broken pores) using SEM on the cross section samples.

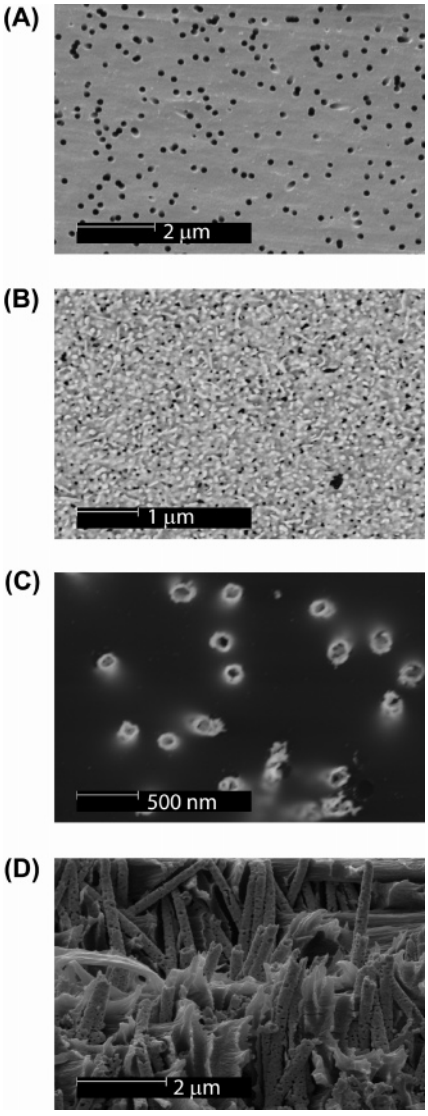

Figure 3. SEM micrograph of NCAMs. (A) Planar image of an uncoated NCAM collected using the SE detector. (B) Planar image of a Au-NCAM collected using the BSE detector. The bright regions on the image indicate where the gold is plated; the dark areas indicate the absence of gold. (C) Planar image of a Au-NCAM collected with the BSE detector after the removal of the gold from the surface. The bright rings on the image depict the gold plated on the pore entries. (D) Cross-sectional SEM image of a Au-NCAM. The cylindrical structures result from gold deposited throughout the pores of the NCAM to form gold nanocapillaries.

Figure 4A, C, and D is images of the inner pore surfaces of Au-NCAMs collected by SEM. As Au-NCAMs prepared by electroless plating may exhibit variable roughness, to minimize the batch-to-batch variability, the samples examined here were from the same electroless plating run. Also, the images were acquired with the same imaging parameters. Au-IgG was used as an indicator to help visualize the immobilized Fab′ inside the gold pores (Au-IgG-Fab′-Au-NCAM: Figure 4A). Detailed immunoreaction procedures for the Fab′-Au with Au-IgG are described in Supporting Information. Figure 4B is a schematic illustration of the immobilized structures inside a single nanocapillary, Au-IgG-Fab′-Au-NCAM. The surface roughness apparent in Figure 4A is due to the 10 nm gold nanoparticles on the IgG tagging reagent. A clean Au-NCAM inner surface (Figure 4C) without modification but cleaned with O_3 as with the other samples before modification and the control Au-

(44) Martin, C. R.; Nishizawa, M.; Jirage, K.; Kang, M. *J. Phys. Chem. B* **2001**, *105*, 1925.

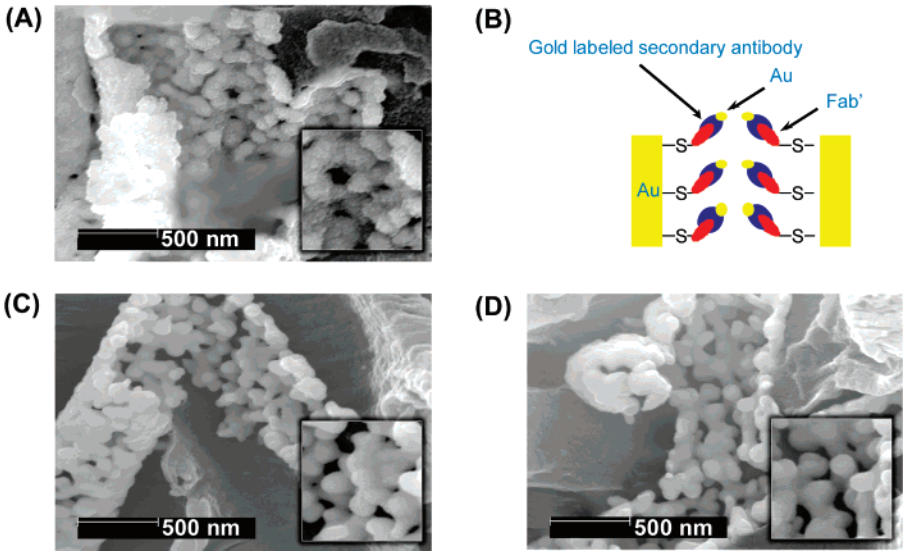

Figure 4. SEM micrographs of the inner pore surfaces of the Au-IgG-Fab′-Au-NCAM and controls. (A) The surface of the pores with the Au-IgG-Fab′-Au-NCAM reveals the granular surface morphology due to the gold particles. (B) Schematic representation of the Au-IgG-Fab′-Au-NCAM, the antibody-based molecular recognition gate A. (C) Clean Au-NCAM without modification. (D) Control Au-NCAM after exposure to the Au-IgG solution after treatment with blocker.

NCAM (Figure 4D) were also examined and support assignment of the surface features to IgG-Au bound to the surface Fab′. The control Au-NCAM was prepared in the same way as the Au-IgG-Fab′-Au-NCAM, except it was not incubated in Fab′ solution before being exposed to Au-IgG. Therefore, the smoother surface of the control as compared to the Au-IgG-Fab′-Au-NCAM mitigates against interpreting the surface roughness in Figure 4A as resulting from nonspecifically adsorbed Au-IgG. Histogram analyses of the intensity of each pixel in the images, thus reflecting morphological differences, show that the Au-IgG-Fab′-Au-NCAM (Figure 4A) has a larger standard deviation ($\sigma = 11$) compared to the clean Au-NCAM (Figure 4C, $\sigma = 6$) and the control Au-NCAM (Figure 4D, $\sigma = 5$). The statistical data were acquired from a small portion of each image (approximately 100×100 nm^2). The inset boxes in the images of Figure 4 were created by capturing a small portion of each corresponding image; magnification and contrast were adjusted in software to emphasize the morphological differences of the image surfaces.

Selective Capture and Release on the Fab′-Au-NCAM. The preceding experiments confirm the ability to immobilize active antibody fragments onto planar Au and Au-NCAMs. Next, the ability of suitably prepared Au-NCAM constructs to selectively capture and release a specific antigen, insulin, from a mixture containing acidic peptide and BSA blocker is tested using MALDI-TOF MS to examine the pore releasates. Acidic peptide was selected as a control antigen because it produces a peak of similar intensity in the mass spectrum when analyzed from an equimolar mixture with insulin, thereby compensating for inherent differences in sensitivity among different analytes.

To prepare the Fab′-Au-NCAM, a Au-NCAM was immersed in Fab′ solution and was incubated for the same amount of time as the Fab′-Au at 4 °C. To remove nonimmobilized Fab′ inside the Au-NCAM pores, the Fab′-Au-NCAM was washed at room temperature (RT) in T/PBS for 15 min on a shaker. The washing step was repeated five times with fresh T/PBS, and the Fab′-Au-NCAM was stored in PBS overnight at 4 °C prior to testing the selective capture and release of specific antigen. Typically, the prepared Fab′-Au-NCAM was used for selective capture and release experiments within 2 days of preparation. Testing of selective capture and release of the specific analyte in Fab′-Au-NCAM constructs was implemented using a method similar to established ELISA protocols, suitably modified to accommodate the format of the Au-NCAM. First, the Fab′-Au-NCAM was incubated in blocker for 1 h at 37 °C followed by incubation in a mixture of 500 nM of *Aplysia* acidic peptide (MW 2960.3; control antigen) and 500 nM of human insulin (MW 5807.6; antigen) prepared in the blocker, 10 mg/mL of BSA in PBS, for 4 h at 37 °C (binding solution). Then, the insulin-Fab′-Au-NCAM was washed at RT in T/PBS for 15 min with shaking (repeated five times with fresh T/PBS) and was stored in PBS overnight at 4 °C to minimize nonspecific adsorption of antigen or control antigen until the on-probe release experiments. To prepare a control sample, a clean Au-NCAM without Fab′ was incubated in blocker for 1 h at 37 °C followed by incubation in binding solution for 4 h at 37 °C. Finally, it was washed and stored as described for the insulin-Fab′-Au-NCAM.

On-probe release of captured insulin from the insulin-Fab′-Au-NCAM was conducted as follows. An approximate 1×1 mm^2 sample of an insulin-Fab′-Au-NCAM was placed on the MALDI target, and 1 μL of releasing buffer and 1 μL of MALDI matrix were applied sequentially. Then, the MALDI target was dried at RT. The on-probe releasate of the control membrane was prepared in the same way.

Figure 5A shows the spectrum of the standard mixture solution of insulin ((ii) m/z 5809.1) and acidic peptide ((i) m/z 2961.5), both at 5 μM; both peaks are of similar intensity at the same concentration. Next, the analyte concentration ability of the Fab′-Au-NCMA assembly was evaluated. A solution containing acidic peptide and insulin at the same concentration as the binding solution (500 nM of each analyte), but without BSA blocker (to circumvent excessively complicated spectrum), was prepared in the antigen-releasing buffer. The MALDI-TOF MS spectrum from a dried droplet of 1 μL solution (0.5 pmole each on the sample spot) was acquired but did not show distinct $[M + H]^+$ analyte peaks (Figure 5B), although the molecular

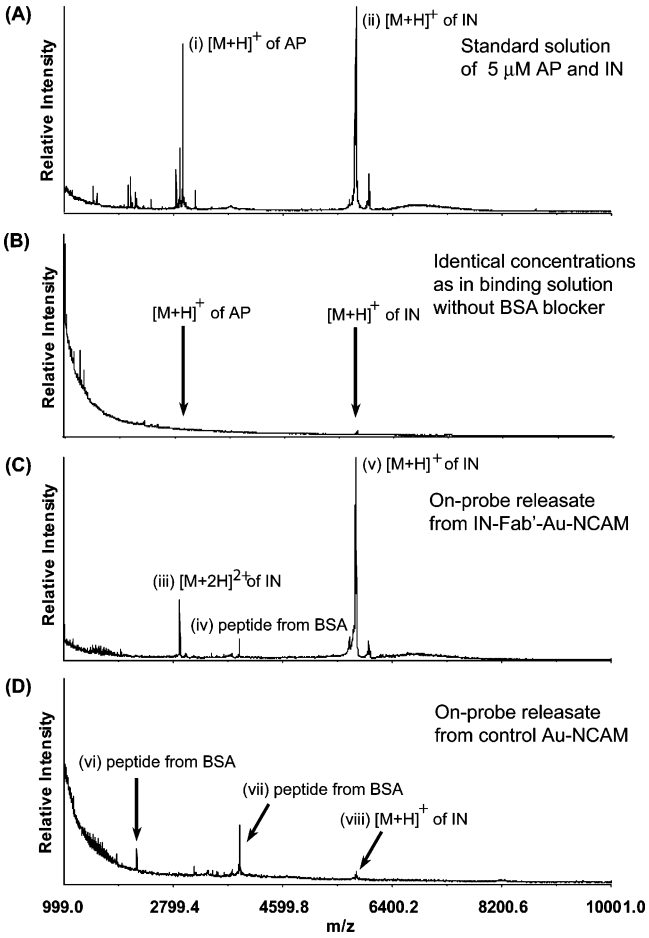

Figure 5. MALDI-TOF MS spectra of a standard solution of 5 μM *Aplysia* acidic peptide (control antigen; acidic peptide, AP) and human insulin (antigen; IN), 5 pmole each on the probe. (A) Spectrum of 500 nM of AP and 500 nM of IN solution prepared in release buffer without BSA blocker, 0.5 pmole each on the probe; (B) on-probe release of captured peptide from the Fab′-Au-NCAM; and (C) on-probe release of captured peptide from (D) the control Au-NCAM. *m*/*z* of peaks are (i) 2961.5, (ii) 5809.1, (iii) 2904.9, (iv) 3886.9, (v) 5809.6, (vi) 2912.3, (vii) 3886.1, and (viii) 5807.1.

ion peaks were persistently sought in multiple spectra. Then, on-probe releasate spectra were acquired by placing a piece of an insulin-Fab′-Au-NCAM on the MALDI target. In contrast to Figure 5B, when the on-probe releasate spectrum of the insulin-Fab′-Au-NCAM was acquired, it easily showed an intense $[M + H]^+$ insulin peak at *m*/*z* 5809.6 (Figure 5C (v)) along with the $[M + 2H]^{2+}$ insulin peak at *m*/*z* 2904.9 (Figure 5C (iii)) and an unassigned peptide peak from the BSA blocker at *m*/*z* 3886.9, consistently. However, no peaks originating from acidic peptide are observed. Comparing the peak intensities of Figure 5B and C, it is clear that the Fab′-Au-NCAM concentrates the specific analyte from the complex mixture. The origin of the unassigned BSA peptide peak was determined by a series of control MS measurements involving releasates from clean Au-NCAMs, BSA-blocked Au-NCAMs, and diluted BSA blocker solutions. (Spectra are available in the Supporting Information.)

Finally, the ability to selectively capture and release a specific analyte from a mixture was examined by comparing the mass spectra of releasate from an insulin-Fab′-Au-NCAM (Figure 5C) and the releasate from the control Au-NCAM (Figure 5D). The MS data indicate that insulin is selectively captured from a peptide mixture and is successfully released by the Fab′-Au-NCAM (Figure 5C). To evaluate the performance of the selective capture and release ability of the antigen on a Fab′-Au-NCAM, the relative intensity ratio of peak (v) to peak (iv) was calculated and averaged across multiple measurements (five spectra for the insulin-Fab′-Au-NCAM and seven spectra for the control Au-NCAM). A 23-fold increase in intensity compared to the control (ratio of (viii) to (vii), Figure 5D) is measured. In this case, peak (iv) and peak (vii) were used as internal references to normalize the data and allow the comparison of the Fab′-Au-NCAM and the Au-NCAM releasate samples in a semiquantitative manner.[45] Details of the statistical analysis are provided in the Supporting Information.

Discussion

We have shown that Fab′ fragments can be effectively immobilized on both planar surfaces and the interior walls of cylindrical nanopores. Although the activity of Fab′ after immobilization onto a solid substrate is not always assured,[21] the protocols used here produced fully functional Fab′ on both surface types. The Fab′ fragments immobilized inside of the Au-NCAMs were competent to sequester and concentrate a selected analyte, insulin in this case, and subsequently release the analyte for offline MS characterization.

The surface coverage of Fab′ is an important parameter to consider when assessing the potential utility of the Fab′-Au-NCAM construct in practical applications, such as a nanoscale molecular sorting. The AFM-derived particle density (Figure 2B) yields a surface coverage $\Gamma_{(Fab')} \sim 9$ fmole/cm^2 (or 0.45 ng/cm^2 for the ~50 kDa Fab′ fragment). For flat surfaces, this is lower than the theoretical maximum. There are three possible explanations for the apparent low coverage. First, part of the reason for the discrepancy between the AFM particle density and the surface coverage of the closest-packed monolayer of immobilized protein, $\Gamma \sim 220-440$ ng/cm,[2,21] results from limitations inherent to the gold particle double-labeling protocol. Because the surface is flat, and Au-IgG is significantly larger than Fab′ (the projected area of a 10 nm gold nanoparticle is ca. 79 nm^2), the double-labeling protocol could significantly underreport the surface coverage. This is consistent with Brogan et al.,[21] who reported that when the captured molecule is significantly larger than the molecule immobilized on the surface, it underrepresents the antigen-binding efficiency and thus underrepresents the surface coverage of the surface-immobilized molecule. Nevertheless, under optimum conditions, double-labeling with 10 nm gold nanoparticles should still be able to obtain coverage up to ~60 ng cm^{-2}. A second factor considers the fact that the double-labeling protocol only reports on fully active surface species. Fab′ fragments, which are bound in a suboptimal orientation, or are partially denatured upon surface binding, would not show up in the assay, thus producing a lower surface-coverage number. Finally, inhomogeneous, in-plane distributions resulting from molecular clustering could also affect the surface coverage assay.

On the other hand, electrolessly plated Au-NCAMs offer high surface areas for immobilization of molecules, not only because of their inner pore areas, but also because of the microscopic roughness of the deposited gold. Wernette et al.[30] reported a 4.4 ± 1.5 increase in the fluorescence intensity of a Pb(II)-sensitive molecular beacon DNAzyme reagent on an electro-

(45) Hattan, S. J.; Parker, K. C. *Anal. Chem.* **2006**, *78*, 7986.

lessly plated gold surface when compared to thermally evaporated planar gold. They ascribed this difference to the microscopic roughness of the electrolessly deposited gold, thereby increasing the effective surface area for DNAzyme binding. Further, Au-NCAMs with 500 nm pores showed a 2.8 ± 0.7 (54% ±14%) increase of fluorescence intensity as compared to blocked pores. Although these are not dramatic increases, they indicate a contribution from immobilization on the inner pore surface. These authors also suggested that larger enhancements could be expected with complete gold deposition throughout the NCAM pores. In our case, the theoretical effective surface area for immobilization of molecules from a piece of 1 × 1 mm^2 Au-NCAM with 200 nm pores is 11.4 mm^2, including head, tail, and inner pore surface areas, but no interior surface roughness, that is, essentially the geometric surface (see Supporting Information for detailed calculations). On the basis of the calculated surface area, an estimated maximum 0.52−1.04 pmole/mm^2 antigen can be captured or released from a Fab′-Au-NCAM construct. However, considering the roughness of the electrolessly plated Au-NCAM (see Figures 3 and 4), we expect the effective binding capacity to be larger. The ability to concentrate analyte from a Fab′Au-NCAM, demonstrated in Figure 5C compared to Figure 5B, is accounted for by a significant amount of active-immobilized Fab′.

We validated this by comparing the release of antigenic and nonantigenic peptides from such surfaces. Because of the inhomogeneous nature of MALDI sample deposition and matrix crystallization, there is variability between mass spectra, even within the same sample spot.[45] Therefore, multiple spectra were acquired from each spot to aid these comparisons. While MALDI is not necessarily quantitative, it can be used for semiquantitation of peptides from similar surfaces,[46] and it can be useful for comparing peak heights for the same peptides between several treatments. The MS measurements demonstrated a large and significant increase in the presence of insulin, the antigenic peptide, as compared to other peptides, after collection and release from the Fab′-Au-NCAM.

Conclusions

This work addresses three specific technical objectives: (a) to develop robust and flexible fabrication strategies for the immobilization of molecular recognition motifs onto the interior surfaces of individual nanocapillaries; (b) to create and implement assays for ligand binding which are sensitive to the intrapore binding events; and (c) to assess whether the ligand-affinity reagent complexes can be released with sufficient control to form the basis for high-efficiency nanoscale affinity separations.

In addition, the fluidic characteristics of the NCAM, combined with the enhanced loading of the molecular recognition element on the high surface area Au-NCAM, contribute to the ability to concentrate and manipulate mass-limited peptide samples. As a generic method, preparation of Fab′-Au-NCAMs is applicable to the broad range of analytes for which a specific antibody is available for the analyte. Incorporating Fab′-Au-NCAM molecular gates into three-dimensional integrated microfluidic architectures provides added functionality to the suite of manipulations already demonstrated using this platform.

One of the key questions to effectively deploying molecular recognition moieties, such as the Pb(II)-sensitive DNAzyme molecular beacon construct,[30,47] surrounds the changes in reactivity that attend immobilization of the reagent on the interior wall of a nanopore. We anticipate that ligand binding in nanometer-scale spaces will be determined by two countervailing tendencies: the increase in wall-collision frequency, Ω_W, of prospective ligands and the reduced volume of phase-space explored because of hindered rotational diffusion, D_R, inside the pore. In the future, the nature of the ligand binding in nanometer-scale spaces will be studied using the Fab′-Au-NCAM. We believe this work will provide a milestone for answering such fundamental questions.

Acknowledgment. This material is based upon work supported by the National Science Foundation under Award No. DMI-0328162 and cooperative agreement CTS-0120978, the Strategic Environmental Research and Development Program under Award No. W9132T-05-2-0028, and the National Institute on Drug Abuse under Award No. DA018310 to the UIUC Neuroproteomics Center on Cell to Cell Signaling. The authors thank S. J. Robinson of the Imaging Technology Group of the Beckman Institute of Advanced Science and Technology at the University of Illinois at Urbana−Champaign for his excellent technical assistance and helpful consultation on SEM imaging. B. Y. Kim appreciates the Korea Science and Engineering Foundation Grant funded by the Korean government (M06-2003-000-10304-0). J-a A. Ho acknowledges the grant support received from the Taiwan National Science Council (NSC 42122F).

Supporting Information Available: Materials and reagents; buffers and MALDI matrix; planar gold substrate preparation for microscopy; electroless gold plating; illustration of the Fab′ preparation procedure with schematic diagram of the antibody structure; microscopic imaging of Fab′-Au surfaces; matrix-assisted laser desorption/ionization time-of-flight mass spectrometry (MALDI-TOF MS); AFM scanning of the Au-IgG-Fab′-Au control surface on ultraflat gold; figure and table of statistical analysis of relative intensity comparison in MALDI-TOF MS spectra; spectra of clean Au-NCAM releasate, BSA blocked Au-NCAM releasate, and diluted BSA blocker solution; the calculation for theoretical effective surface area of 1 × 1 mm^2 of Au-NCAM. This material is available free of charge via the Internet at http://pubs.acs.org.

JA070041W

(46) Wang, Q.; Jakubowski, J. A.; Sweedler, J. V.; Bohn, P. W. *Anal. Chem.* **2004**, *76*, 1.

(47) Swearingen, C. B.; Wernette, D. P.; Cropek, D. M.; Lu, Y.; Sweedler, J. V.; Bohn, P. W. *Anal. Chem.* **2005**, *77*, 442.